Basic Evidence of the Molecular Dispersion of $MnCeO_x$ Catalysts Synthesized via a Novel "Redox-Precipitation" Route

Francesco Arena,*[,†,‡] Giuseppe Trunfio,[†] Jacopo Negro,[†] Barbara Fazio,[§] and Lorenzo Spadaro[‡]

Dipartimento di Chimica Industriale e Ingegneria dei Materiali, Università degli Studi di Messina, Salita Sperone 31 c.p. 29, I-98166 S. Agata, Messina, Italy, Istituto CNR-ITAE "Nicola Giordano", Salita S. Lucia 39, I-98126 S. Lucia, Messina, Italy, and Istituto di Processi Chimico-Fisici del CNR (CNR-IPCF) di Messina, Via G. La Farina 237, I-98123 Messina, Italy

Received January 22, 2007

A novel synthesis route driving redox-precipitation reactions among Mn^{VII}, Ce^{III}, and Mn^{II} precursors in basic aqueous solution yields $MnCeO_x$ catalysts (Mn_{at}/Ce_{at}, 0.33−2.0) with a (quasi)molecular dispersion of the active phase and enhanced textural properties in comparison to the conventional coprecipitation method. The basic characteristics of the redox-precipitation process leading to a solid architecture missing a substantial "long-range" crystalline order are discussed. With an excellent reproducibility and irrespective of the Mn_{at}/Ce_{at} ratio, the redox-precipitation method also ensures unchanged textural, structural, and chemical properties of the $MnCeO_x$ catalysts. As a much improved dispersion of the active phase, the redox-precipitation route greatly promotes the redox behavior and the surface affinity toward gas-phase oxygen of the $MnCeO_x$ system.

Introduction

Environmental catalysis is a rapidly growing field of both academic and technological interest pressed by the basic need to preserve natural resources and human health. On this account, a variety of chemical processes aimed at removing noxious organic pollutants both in gas exhausts and in wastewater, mostly based on total catalytic oxidation reactions, are under scrutiny worldwide.

Although a very broad range of reaction targets and conditions does not allow the assessment of some general rules on environmental catalyst requirements yet, according to theoretic principles of oxidation catalysis,[1,2] an enhanced surface mobility and availability of oxygen atoms constitutes a necessary condition for driving a deep oxidative conversion of organic substrates to carbon dioxide.

A potential alternative to high-cost noble metals as total oxidation catalysts,[1−5] for several decades the $MnCeO_x$ system has attracted a great deal of research interest as its noticeable performance in the catalytic wet oxidation (CWO) of wastewaters with air/oxygen,[3−12] the catalytic combustion of volatile organic carbons (VOCs),[13−20] and the selective reduction of NO_x's.[21,22] Generally, a superior catalytic behavior has been associated with an enhanced reducibility of "dispersed" manganese ions with higher average oxidation numbers (AON),[4−13,16,20−23] while the reversibility of the surface redox cycle is critical for catalyst stability.[6−9,14] A proper "tuning" of the structural and electronic features of the active phase is then a benchmark for the catalytic pattern of the $MnCeO_x$ system.[4−11,20−23] In particular, affecting the texture and the active phase dispersion, which control nature and extent of oxide−support interaction,[4−8,10−13,20−23] the preparation method[4,5,9,11,17−23] and promoters' addition[5−10,13,17]

* To whom correspondence should be addressed at Università di Messina. Tel.: +39 090 6765606. Fax: +39 090 393134. E-mail: francesco.arena@unime.it.
† Università degli Studi di Messina.
‡ Istituto CNR-ITAE "Nicola Giordano".
§ Istituto di Processi Chimico-Fisici del CNR (CNR-IPCF) di Messina.

(1) Bielañski, A.; Haber, J. *Oxygen in Catalysis;* Marcel Dekker, Inc.: New York, 1991.
(2) Sokolovskii, V. *Catal. Rev. Sci. Eng.* **1990**, *32*, 1.
(3) Matatov-Meytal, Y. I.; Sheintuch, M. *Ind. Eng. Chem. Res.* **1998**, *37*, 309.
(4) Imamura, S. In *Catalysis by Ceria and Related Materials*; Trovarelli, A., Ed.; Imperial College Press: London, U.K., 2002; Vol. 14, p 431.
(5) Bhargava, S. K.; Tardio, J.; Prasad, J.; Foger, K.; Akolekar, D. B.; Grocott, S. C. *Ind. Eng. Chem. Res.* **2006**, *45*, 1221.
(6) Chen, H.; Sayari, A.; Adnot, A.; Larachi, F. *Appl. Catal. B* **2001**, *32*, 195.
(7) Hamoudi, S.; Larachi, F.; Sayari, A. *J. Catal.* **1998**, *177*, 247.
(8) Hussain, S.T.; Sayari, A.; Larachi, F. *Appl. Catal. B.* **2001**, *34*, 1.
(9) Abecassis-Wolfovich, M.; Jothiramalingam, R.; Landau, M. V.; Herrskowitz, M.; Viswanathan, B.; Varadarajan, T. K. *Appl. Catal. B* **2005**, *59*, 91.
(10) Arena, F.; Parmaliana, A.; Trunfio, G. *Proceedings of the TOCAT 5 Conference*, Tokyo, July 23−28, 2006: in press.
(11) Kim, S. K.; Ihm, S. K. *Top. Catal.* **2005**, *33* (1−4), 171.
(12) Silva, A. M. T.; Marques, R. R. N.; Quinta-Ferreira, R. M. *Appl. Catal. B* **2004**, *47*, 269.
(13) Terribile, D.; Trovarelli, A.; de Leitnburg, C.; Primavera, A.; Dolcetti, G. *Catal. Today* **1999**, *47*, 133.
(14) Cracium, R. *Catal. Lett.* **1998**, *55*, 25.
(15) Liu, Y.; Luo, M.; Whei, Z.; Xin, Q.; Ying, P.; Li, C. *Appl. Catal. B* **2001**, *29*, 61.
(16) Gil, A.; Gandía, L. M.; Korili, S. A. *Appl. Catal. A* **2004**, *274*, 229.
(17) Li, W. B.; Chu, W. B.; Zhang, M.; Hua, J. *Catal. Today* **2004**, *93*−*95*, 205.
(18) Lamaita, L.; Peluso, M. A.; Sambeth, J. E.; Thomas, H. J. *Appl. Catal. B* **2005**, *61*, 114.
(19) Barrio, I.; Legórburu, I.; Montes, M.; Domínguez, M. I.; Centeno, M. A.; Odriozola, J. A. *Catal. Lett.* **2005**, *101* (3−4), 151.
(20) Tang, X.; Li, Y.; Huang, X.; Hu, Y.; Zhu, H.; Wang, J.; Shen, W. *Appl. Catal. B* **2006**, *62*, 265.
(21) Imamura, S.; Shono, M.; Okamoto, N.; Hamada, A.; Ispida, S. *Appl. Catal. A* **1996**, 142, 279.
(22) Qi, G.; Yang, R.T. *J. Catal.* **2003**, *217*, 434.
(23) Adachi, G.-Y.; Masui, T. In *Catalysis by Ceria and Related Materials*; Trovarelli, A., Ed.; Imperial College Press: London, U.K., 2002; Vol. 3, p 51.

10.1021/cm070198n CCC: $37.00
Published on Web 03/28/2007

Table 1. List of the Studied Catalysts

catalyst	Mn_{at}/Ce_{at}[a] design	Mn_{at}/Ce_{at}[a] experimental	[Mn] (wt %)	preparation method	T_{calc}[b] (K)	SA_{BET} (m^2/g)	PV (cm^3/g)	APD[c] (Å)
M1C3-R	0.33	0.33	9.1	red.-prec.		244	0.31	32
M1C3-R4	0.33	0.33	9.1	red.-prec.	673	143	0.20	33
M3C4-R	0.75	0.71	16.7	red.-prec.		255	0.53	63
M3C4-R4	0.75	0.71	16.7	red.-prec.	673	169	0.47	70
M1C1-R	1.00	0.95	20.5	red.-prec.		219	0.61	84
M1C1-R4	1.00	0.95	20.5	red.-prec.	673	154	0.49	85
M3C2-R	1.50	1.44	26.7	red.-prec.		208	0.62	96
M3C2-R4	1.50	1.44	26.7	red.-prec.	673	157	0.45	79
M2C1-R	2.00	2.13	32.8	red.-prec.		244	0.59	74
M2C1-R4	2.00	2.13	32.8	red.-prec.	673	140	0.50	105
M1C1-PC4[d]	1.00	1.00	21.2	co-prec.	673	101	0.24	94
M1C1-PN4[e]	1.00	0.94	20.4	co-prec.	673	72	0.31	162

[a] Atomic ratio from design and XRF measurements, respectively. [b] Calcination temperature (6 h). [c] Average pore diameter. [d] From $CeCl_3-MnCl_2$ precursors. [e] From $Ce(NO_3)_3-Mn(NO_3)_2$ precursors.

are very crucial issues for improving the reactivity of the title system.

Therefore, this paper aims at showing that a new synthesis route, driving redox-precipitation reactions among various Mn and Ce precursors in basic aqueous solution, leads to molecularly dispersed $MnCeO_x$ catalysts in a very wide range of the Mn loading (9−33 wt %). With an excellent reproducibility, the new synthesis method allows improving the structure, the morphological properties, and the redox behavior of $MnCeO_x$ catalysts in comparison to the conventional coprecipitation method.

Experimental Section

$MnCeO_x$ Catalysts. $MnCeO_x$ catalysts with different chemical composition (Mn_{at}/Ce_{at}, 0.33−2.10) were prepared via the new "redox-precipitation" route, according to the following procedure.[24,25] An amount of the $KMnO_4$ precursor, in a 10% stoichiometric excess, dissolved in deionized water was titrated at 333 K under vigorous stirring with a solution of $Ce(NO_3)_3$ and $Mn(NO_3)_2$ precursors, keeping constant the pH (8.0 ± 0.3) by the addition of a 0.2 M KOH solution. After titration, the solid was digested for 30 min at 333 K and then filtered, repeatedly washed with hot distilled water, and dried overnight at 373 K. Aliquots of the dried samples were further calcined in air at 673 K (6 h).

For the sake of comparison, reference $MnCeO_x$ catalysts (Mn_{at}/Ce_{at}, 1.0) were prepared by the coprecipitation routes, using $Mn(NO_3)_2-Ce(NO_3)_3$ (M1C1-PN4) or $MnCl_2-CeCl_3$ (M1C1-PC4) precursors and, in both cases, a 10% Na_2CO_3 solution as precipitant.[6−10,14,23] The solids were dried at 373 K (16 h) and then calcined in air at 673 K (6 h).

The list of the studied samples and the relative physicochemical properties are presented in Table 1.

Surface Area and Pore Size Distribution. Surface area (SA_{BET}) and the pore size distribution (PSD) were obtained from the nitrogen adsorption/desoprtion isotherm at 77 K using a fully automated ASAP 2010 (Micromeritics Instruments) gas adsorption system. The isotherms were elaborated according to the BET method for calculation of the surface area, while the Horvath−Kavazoe and BJH methods were employed for "micro-" and "meso-" PSD evaluation, respectively.

X-ray Diffraction. X-ray diffraction (XRD) analysis of powdered samples was performed in the 2θ range 20−75° with a scan step size of 0.05°/s using a Philips X-Pert diffractometer operating with a Ni β-filtered Cu Kα radiation at 40 kV and 30 mA. The ceria average particle size was calculated by the Sherrer's equation.

Transmission Electron Microscopy. Transmission electron microscopy (TEM) analysis of the catalysts was performed using a PHILIPS CM12 microscope (point-to-point resolution, 3 Å) on catalyst samples ultrasonically dispersed in isopropanol and deposited over a thin carbon film supported on a standard copper grid.

X-ray Photoelectron Spectroscopy. X-ray photoelectron spectroscopy (XPS) data were obtained by a Physical Electronics GMBH PHI 5800-01 spectrometer, using a monochromatized Al Kα radiation at power beam of 350 W and pass energy of 60 eV. The binding energy regions investigated were 635−680 eV (Mn 2p), 280−300 eV (C 1s), 525−540 eV (O 1s), and 870−935 eV (Ce 3d) using the C 1s line (284.8 eV) of adventitious carbon as reference.

Temperature Programmed Reduction. Temperature programmed reduction (TPR) measurements in the range 273−1073 K were carried out using a 6% H_2/Ar mixture flowing at 60 stp mL min^{-1} into a linear microreactor (d_{int}, 4 mm) containing a catalyst sample of approximately 30 mg heated at the rate of 12 K·min^{-1}. TPR measurements were performed without any pretreatment of the "as-prepared" samples or after an in situ pretreatment at 673 K for 30 min in a pure oxygen flow (30 stp mL min^{-1}).

Micro-Raman Spectroscopy. Micro-Raman spectra were obtained at room temperature in back scattering geometry. The excitation source was a He−Ne laser (632.8 nm line) focused on the sample with a microscope (50× magnification objective) with an incident power of approximately 3 mW. The scattered light was collected by the same microscope, dispersed by a HR460 monochromator (Horiba-Jobin Yvon), and detected by a charge-coupled device array sensor at 77 K. The spectral resolution in the experiments is 3 cm^{-1}.

Results and Discussion

(1) Aims and Strategy for Design of the New Synthesis Route. The aim of maximizing the dispersion of the active phase to enhance the redox activity for getting an improved CWO performance[4−13] has necessitated the design of an alternative synthesis route of the $MnCeO_x$ system accomplishing a mix of the oxide components at an "atomic" level. This is to overcome the major drawback of the conventional coprecipitation technique leading, as a rule, to mixtures of "monophase" precipitate particles because of

(24) Arena, F.; Trunfio, G.; Negro, J.; Spadaro, L. *Mater. Res. Bull.* **2006**, submitted.
(25) Arena, F.; Negro, J.; Parmaliana, A.; Spadaro, L.; Trunfio, G. *Ind. Eng. Chem. Res.* **2007**, submitted.

different precipitation kinetics of each cation.[22] Therefore, a "selective" cogeneration of the precipitating phases to further control "specific" interactions among proper precursors was the main objective of the new synthesis design. Preliminary experiments allowed that the precipitation of Ce^{3+} and Ce^{4+} cations (10^{-3} M) as hydroxide/oxides occurs at pH values of 8.4 and 3.1, corresponding to K_{ps} values of 1.6×10^{-20} and 2.5×10^{-47} for $Ce(OH)_3$ and $Ce(OH)_4$, respectively, while a K_{ps} value of 1.5×10^{-13} has been found for the $Mn(OH)_2$ species to be ascertained.[26] Then, redox reactions of MnO_4^- with $Ce^{3+}-Mn^{2+}$ ions in basic solution were devised to attain a simultaneous precipitation of the MnO_2 and CeO_2 species and a "molecular mixing" of the oxide species. Namely, the $KMnO_4$ precursor ($\approx$10 g/L) was titrated with a solution of Ce^{3+} and Mn^{2+} ions at constant pH (8.0 ± 0.3), to drive the following reactions:

$$MnO_4^- + 3e^- + 2H_2O \rightarrow MnO_2(\downarrow) + 4HO^- \quad (1)$$

$$Mn^{2+} + 4HO^- \rightarrow MnO_2(\downarrow) + 2e^- + 1H_2O \quad (2)$$

$$Ce^{3+} + 4HO^- \rightarrow CeO_2(\downarrow) + e^- + 2H_2O \quad (3)$$

Considering the concentration of the MnO_4^-, Mn^{2+}, Ce^{3+}, Ce^{4+}, and OH^- species and above K_{ps} values for a catalyst with a nominal Mn_{at}/Ce_{at} ratio of 1, the redox potentials of the above reactions (+0.57 V (eq 1); −0.39 V (eq 2); and −0.255 V (eq 3)) confirm that the oxidation of the Ce^{3+} and Mn^{2+} cations by MnO_4^- precursor should proceed owing to a "cell-concentration" effect. This approach matches the core issue of design, as the formation of the precipitated species occurs only further to "direct" and "selective" molecular interactions between the oxidant and the reducing species.

With a lower limit in terms of the Mn_{at}/Ce_{at} ratio equal to 0.33 (e.g., $mol_{Mn^{II}} = 0$), the designed catalyst was obtained by dosing the amount of the various precursors (see Experimental Section) according to the quantitative relationships provided by the following equation system

$$3mol_{Mn^{VII}} = 2mol_{Mn^{II}} + mol_{Ce^{III}} \quad (a)$$

$$\frac{mol_{Mn^{VII}} + mol_{Mn^{II}}}{mol_{Ce^{III}}} = \left(\frac{Mn_{at}}{Ce_{at}}\right)_{design} \quad (b)$$

$$mol_{Mn^{VII}} + mol_{Mn^{II}} + mol_{Ce^{III}} = 1 \quad (c)$$

referring to electron (a) and mass (c) balances and the designed catalyst composition (b), respectively.

(2) Structural Properties. A first preliminary evidence of the peculiar structural features induced by the "redox-precipitation" technique stems from a comparison of the surface area values (Table 1), because all the "redox-precipitated" samples are characterized by a much larger surface exposure in the calcined (140−160 m^2/g) and mostly in the dried form (220−250 m^2/g) than the coprecipitated ones (70−100 m^2/g). Favoring a remarkable development of surface area, even larger than that so far reported for similar systems,[4−12,18,20,23] the "redox-precipitation" process moreover ensures a solid texture not depending on the Mn_{at}/Ce_{at} ratio, while this is a very critical parameter for any other preparation methods.[5−10,18−23]

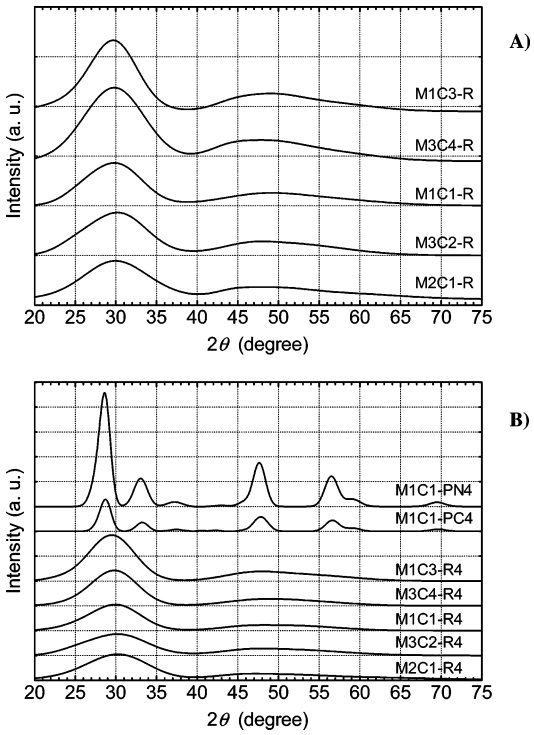

Figure 1. XRD patterns of the dried (A) and calcined (B) $MnCeO_x$ catalysts.

Then, the XRD technique was used to attain comparative information on the structural characteristics of both dried (Figure 1A) and calcined (Figure 1B) catalysts. Irrespective of composition (e.g., Mn_{at}/Ce_{at}, 0.33−2.0) and calcination treatment (673 K), the XRD patterns confirm the peculiarity of the $MnCeO_x$ catalysts synthesized via the "redox-precipitation" route. The diffractograms of the dried samples look in fact quite atypical (Figure 1A), consisting of a broad and "smoothed" component spanned in the 2θ range 20−38° and another less intense signal in the range 40−60°, denoting the lack of a significant "long-range" crystalline order. Even if the uncalcined systems are characterized by analogous, very high surface area values (Table 1), such peculiar XRD patterns mirror a "disordered" arrangement, consequent not only to the "soft" thermal treatment (e.g., drying at 373 K). Indeed, despite an evident decrease in surface area (Table 1) indicating some incipient structural rearrangement, the XRD patterns of the calcined M*x*C*y*-R4 samples (Figure 1B) are practically identical to those of the "dried" ones (Figure 1A). A systematic decrease of the intensity with the Mn_{at}/Ce_{at} ratio suggests that these components are mostly related to the ceria carrier,[14,24,25,27,28] according to the fact that similar diffractograms have been recorded for extremely dispersed ceria systems,[14,27−29] characterized by a surface-to-total cerium ions ratio close to 100%.[29] Therefore, the diffractograms of "redox-precipitated" catalysts monitor a high spatial anysotropy, resulting from

(26) Kolthoff, I. M.; Sandell, E. B.; Mehan, E. J.; Bruckenstein, S. *Quantitative Analytical Chemistry*; Piccin Edition: Padua, Italy, 1973; Vol. 1, p 268.

(27) Cracium, R. *Solid State Ionics* **1998**, *110*, 87.

(28) Zheng, X.; Wang, S.; Wang, X.; Wang, S.; Wang X.; Wu, S. *Mater. Lett.* **2005**, *59*, 2769.

(29) Tsunekawa, S.; Sivamohan, R.; Ito, S.; Kasuya A.; Fukuda, T. *Nanostruct. Mater.* **1999**, *11*, 141.

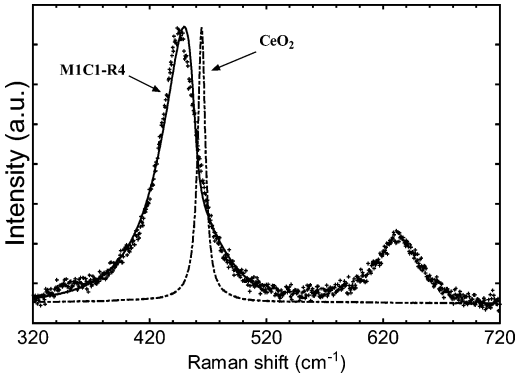

Figure 2. Comparison of the Raman spectrum of a crystalline ceria sample with that of the M1C1-R4 catalyst. The solid line is the fitting curve from the model reported in the ref 36.

"sticking" of MnO_x and CeO_2 species at a (quasi)molecular level, whereas the inadequacy of the conventional coprecipitation route in getting an effective mixing of the oxide components is confirmed by different XRD patterns, denoting the presence of crystalline phases in both M1C1-PN4 and M1C1-PC4 samples (Figure 1B). Besides the typical diffraction lines of the cerianite, small resolved reflexes at 37.3 and 42.4° signal in fact an incipient crystallization of the MnO_x mostly in the form of pyrolusite.[6−8,16,17,25,30] Then, a mean ceria particle size of 5.0−5.5 nm is calculated from the ⟨200⟩ peak for the M1C1-PC4 and M1C1-PN4 systems, in agreement with the surface exposure (Table 1).[4−9,23]

The Raman spectrum of the representative M1C1-R4 sample is compared with that of the CeO_2 single crystal in Figure 2. According to literature data,[31,32] the Raman spectrum of a fluorite ceria structure is dominated by a main band centered at 462−466 cm^{-1} due to the F_{2g} active mode (triply degenerate), which is very sensitive to the crystal symmetry. This scattering contribution can be viewed as a symmetric breathing mode of oxygen atoms around cerium ions.[32] A much smaller component at approximately 590 cm^{-1}, due to the nondegenerate Raman inactive LO mode, can be recorded for microcrystalline ceria samples, these being caused by a perturbation of the local M−O bond symmetry which leads to the relaxation of the symmetry selection rules.[31,32] Mostly generated by oxygen vacancies in the ceria lattice, this band increases as the ceria particle gets smaller,[31−32] its absence in the spectrum of the ceria sample accounting for the high degree of crystallinity of the reference material. On the other hand, the F_{2g} mode of the M1C1-R4 sample is strongly shifted to lower frequency (peak position at ca. 440 cm^{-1}) and slightly asymmetric (Figure 2), accounting for a very small size of crystalline domains. Matching with the symmetric Mn−O vibrations of the MnO_6 group,[33,34] the peak centered at approximately 630 cm^{-1} is instead the Raman contribution of the MnO_x species. Position

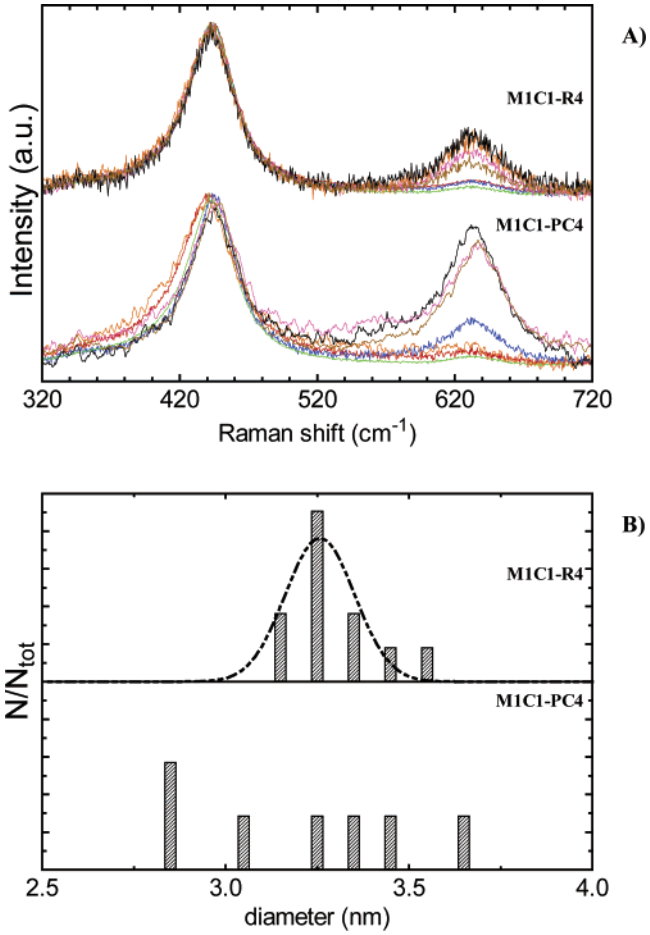

Figure 3. (A) Raman spectra normalized to the ceria F_{2g} mode recorded at several points of the M1C1-R4 and M1C1-PC4 samples. (B) Ceria particle size distribution of the M1C1-R4 and M1C1-PC4 samples obtained by the analysis of the spectra in part A according to ref 36.

and intensity of this band allow the small component at 590 cm^{-1} of the ceria lattice to be hardly, if at all, detectable.

Then, Raman spectra were recorded at several points to test the "local" homogeneity of the M1C1-PC4 and M1C1-R4 samples, their comparison being shown in Figure 3A. The M1C1-R4 sample features a rather constant position (440 cm^{-1}) and line width (41.5 ± 2.0 cm^{-1}) of the ceria F_{2g} Raman peak, while the component relative to MnO_x species, though keeping unchanged its center position (≈630 cm^{-1}), has a relative intensity variable between approximately 4 and 30%. The M1C1-PC4 sample presents the same main features at 440 and 630 cm^{-1}, as a result of the F_{2g} mode of ceria and MnO_x species, respectively. Although the position of the former band indicates the presence of nanosized ceria domains also in this sample, the line width is much more variable (42 ± 7.5 cm^{-1}), and also the relative intensity of the MnO_x component varies in a much greater range (5−80%). Despite similar spectral features, Raman data indicate that the "redox-precipitated" sample has a much more homogeneous chemical composition and ceria particle size distribution than the coprecipitated one.

It is well-known that several factors can contribute to the change in Raman position and line width of the F_{2g} mode, including grain size and morphology.[31,32] In general, inhomogeneous strain and phonon confinement are responsible for the broad and asymmetric character of the band as the

(30) Arena, F.; Torre, T.; Raimondo C.; Parmaliana, A. *Phys. Chem. Chem. Phys.* **2001**, *3*, 1911.
(31) Reddy, B. M.; Khan, A. *Catal. Surv. Asia* **2005**, *9*, 155.
(32) McBride, J. R.; Hass, K. C.; Poindexter, B. D.; Weber, W. H. *J. Appl. Phys.* **1994**, *76*, 2435.
(33) Jiang J.; Kucernak A. *Electrochim. Acta* **2002**, *47*, 2381.
(34) Ammundsen, B.; Burns, G. R.; Islam, M. S.; Kanoh, H.; Rozière, J. *J. Phys. Chem. B* **1999**, *103*, 5175.

particle size gets smaller. In an ideal crystal, the translational symmetry leads to an infinite spatial correlation function of the phonon and, as a consequence, to plane wave phonon eigenstates; the momentum selection rules allow only the phonons with $q = 0$ to be active in first-order Raman scattering, where q is the phonon wave vector. In the presence of strains, defects, and "finite size" effects, however, the selection rules can partially relax; in nanocrystals, in fact, also the phonons with $q \neq 0$ can give contribution to first-order Raman scattering, causing the broadening and the red shift of the Raman band. A phenomenological model to deduce the nanocrystals size (L) from the Raman spectrum was developed by Richter et al.[35] and subsequently improved by Campbell and Fauchet for the case of strongly confined phonons.[36] This model takes into account a Gaussian spatial correlation as the weighting function for the amplitude of the wave function of the off-center phonons in low-dimensional materials. We used this approach to fit our experimental data, and we expressed the Raman intensity $I(\omega)$ as follows

$$I(\omega) \propto \sum_{i=1}^{3} \int_0^1 \frac{\exp(-q^2L^2/4)\, d^3q}{[\omega - \omega_i(q)]^2 + (\Gamma_0/2)^2}$$

where q is in $2\pi/a$ (with the lattice constant $a = 0.541$ nm for cerium oxide), L is in units of a, and $\Gamma_0 = 10$ cm^{-1} (the "natural" line width of the ceria F_{2g} mode). In the relation, the sum over the three branches of phonon dispersion ($\omega_i(q)$)[37] is due to the loosening of the triple degeneration of the F_{2g} mode when $q \neq 0$. The good agreement between the fitting curve and the experimental data is evident from Figure 2. The negligible variations of the F_{2g} line width for the M1C1-R4 sample (Figure 3A) results in a very narrow Gaussian particle size distribution centered at 3.25 nm (Figure 3B), while much stronger changes of that component for the coprecipitated sample (Figure 3A) account for a featureless size distribution spanned in the range 2.5−4.0 nm (Figure 3B), in satisfactory agreement with the size value (ca. 5 nm) previously quoted by XRD analysis.

Further insights into the influence of the preparation method on the structural features of MnCeO$_x$ catalysts are available from TEM images of the representative M1C1-PC4 (A, B), M1C1-R4 (C, D), and M1C1-R (E, F) catalysts shown in Figure 4. The coprecipitated system consists of large and "closely packed" agglomerates of "stepped" particles (5−10 nm) with an irregular morphology (Figure 4A). At high magnification (Figure 4B), the sample appears as an intricate array of randomly and "stepped" crystalline domains (5−10 nm), characterized by the presence of ordered fringes with an estimated interatomic distance of 3.2 Å, typical of crystalline ceria.[26] Although the morphology of aggregates is not too dissimilar from that of the coprecipitated sample, the dried (Figure 4E) and calcined (Figure 4C) "redox-precipitated" samples look less densely "packed". Moreover, a sporadic presence of small crystalline domains,

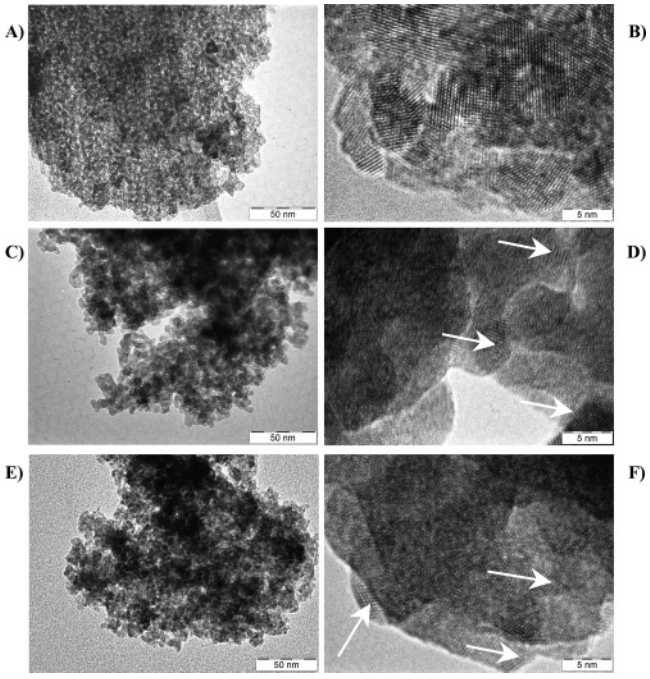

Figure 4. TEM micrographs of the M1C1-PC4 (A, B), M1C1-R4 (C, D), and M1C1-R (E, F) catalysts at low (A, C, E, ×99 000) and high (B, D, F, ×920 000) magnification.

randomly dispersed into a prevalently "amorphous" matrix, renders ceria poorly evident at high magnification (Figure 4D,F). Considering a very irregular shape of such domains, a rough size on the order of a few (3−5 nm) nanometers can be estimated.

Therefore, the basic information of characterization finding is that the MnO$_x$ and CeO$_2$ phases in "redox-precipitated" catalysts are mixed at a quasi-molecular level, forming a prevalently amorphous structure "embedding" small concentrations of nanosized ceria domains, whereas the coprecipitated catalysts mostly retain the typical features of a "conventional" (micro)crystalline material.

(3) Textural and Morphological Properties. The "sticking" of the MnO$_x$ and CeO$_x$ molecules, selectively prompted by the electron transfer between MnO_4^- and Ce^{3+}/Mn^{2+} species (see supra), leads to a very reproducible solid "architecture", peculiar characteristic of the "redox-precipitation" technique. In fact, a mechanism of solid formation fairly different from that occurring in any other synthesis routes could allow a catalyst texture independent from chemical composition (Table 1).[5−10,12,20−23] In fact, the PSD curves in Figure 5 show that the dried M3C4-R (Figure 5A) and M1C1-R (Figure 5B) samples have an analogous PSD, almost entirely spanned in the range 10−100 Å, with a pronounced maximum between 60 and 100 Å. These account for analogous cumulative curves and pore volume values (Table 1). Such a "constant" texture stems from the "same" interaction path of precursors generating composite MnCeO$_x$ *nano*particles which, aggregating, form a porous network with a size distribution comparable with that of the same particles. In spite of the surface area decrease, the calcined samples retain an analogous porous structure as indicated by the PSD of the M1C1-R4 sample (Figure 5C) showing only a slight shift of the maximum position (70−110 Å). With a "regular" weight loss (<20%) in the range 293−873

(35) Richter, H.; Wang, Z. P.; Ley, L. *Solid State Commun.* **1981**, *39*, 625.
(36) Campbell, I. H.; Fauchet, P. M. *Solid State Commun.* **1986**, *58*, 739.
(37) Patil, S.; Seal, S.; Guo, Y.; Schulte, A.; Norwood; J. *Appl. Phys. Lett.* **2006**, *88*, 243110.

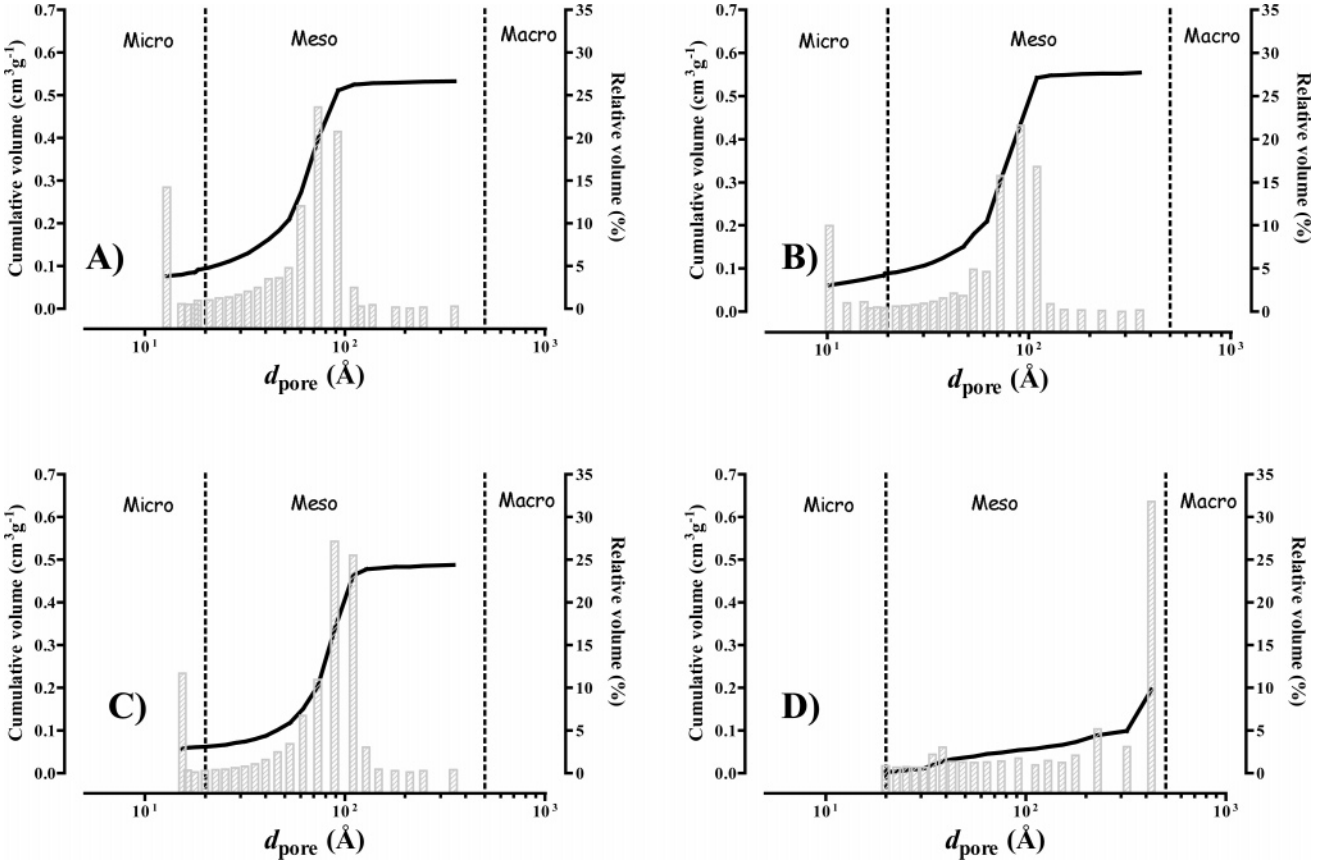

Figure 5. PSD of the M3C4-R (A), M1C1-R (B), M1C1-R4 (C), and M1C1-PC4 (D) catalysts.

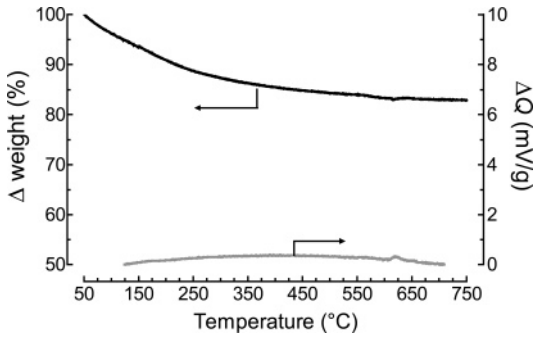

Figure 6. TGA-DSC data of the M1C1-R sample in air.

K, mostly due to an ongoing dehydroxylation process, the thermogravimetric analysis/differential scanning calorimetry (TGA-DSC) curves of the M1C1-R sample (Figure 6) confirm that calcination does not yield any important phase-reconstructuring (Figure 1) and, thus, the surface area and pore volume decrease is due to a closer "packing" with minor effects on PSD and APD (Table 1).

On the contrary, the coprecipitated M1C1-PC4 sample, characterized by much lower surface area (101 m^2/g) and pore volume (0.24 cm^3/g) values, features a "flat" PSD spanned in the whole range of 10−500 Å with a sharp maximum at the highest end, accounting for approximately 30% of the total void fraction (Figure 5D). This different texture is a consequence of the "chaotic" proceeding of nucleation-growth processes in the coprecipitation route,[23] leading to formation of fairly different sized "mono-oxide" particles which, aggregating, form a porous structure with a broad random size distribution.

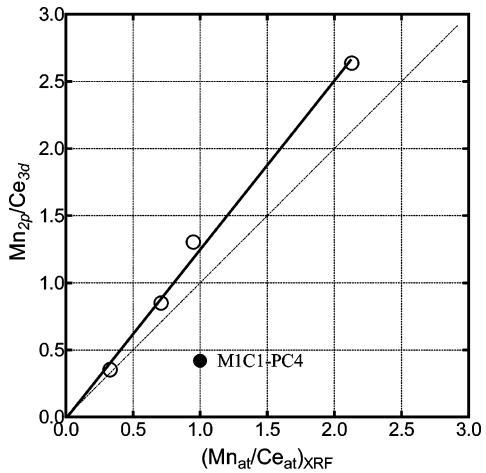

Figure 7. Surface manganese-to-cerium atomic ratio from Mn 2p/Ce 3d signals (XPS) ratio vs the bulk (X-ray fluorescence, XRF) atomic composition of the calcined "redox-precipitated" (○) and "coprecipitated" M1C1-PC4 (●) catalysts.

Furthermore, XPS measurements have been carried out to shed light into the effects of the preparation method and manganese loading on surface composition and dispersion of the calcined catalysts. In particular, the XPS data of the "redox-precipitated" catalysts in terms of the surface Mn/Ce atomic ratio (e.g., Mn 2p/Ce 3d) are compared with the bulk composition data (Table 1) in Figure 7. A very accurate straight-line relationship is diagnostic of a constant degree of dispersion of Mn ions and, although a slope value (1.26) larger than one could signal some surface segregation of the active phase, this finding is consistent with a "monolayer" dispersion of the active phase. Considering the wide range

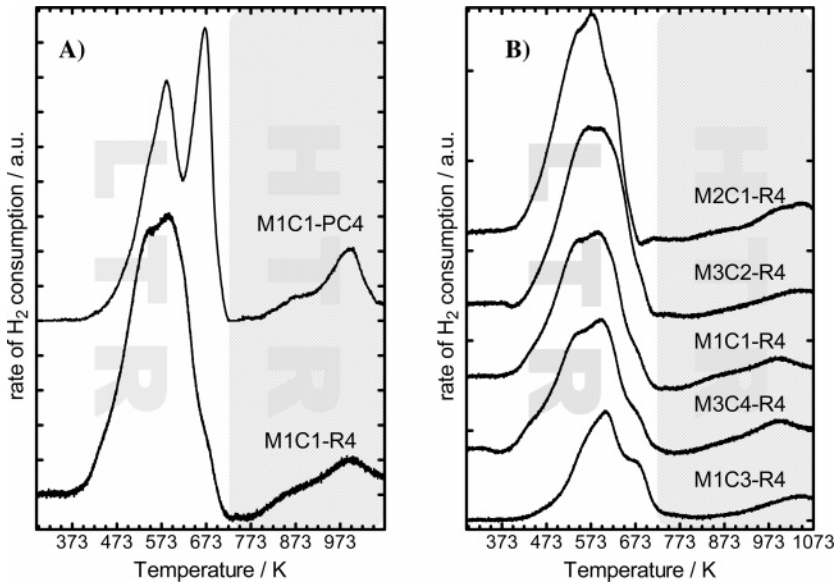

Figure 8. (A) Influence of the preparation method on the TPR profile of M1C1-R4 and M1C1-PC4 catalysts (Mn/Ce, 1.0). (B) Effect of the Mn/Ce atomic ratio on the TPR profile of the calcined "redox-precipitated" catalyst.

Table 2. TPR Data of the Calcined (673 K) MnCeO$_x$ Catalysts

							H_2 consumption		
sample	$T_{0,red}$ (K)	T_{M0} (K)	T_{M1} (K)	T_{M2} (K)	T_{M3} (K)	T_{M4} (K)	(mmol/g$_{cat}$)[a]	(mmol/g$_{cat}$)[b]	H_2/Mn[c]
M1C3-R4	390			586	673	1023	2.30	1.94	1.16
M3C4-R4	375		540	591		989	3.52	2.95	0.93
M1C1-R4	365		545	591		998	3.60	3.27	0.85
M3C2-R4	365		568	599		1050	3.94	3.78	0.77
M2C1-R4	375		550	573	645	1035	5.27	4.60	0.79
M1C1-PC4	400			588	673	1000	3.31	2.71	0.70
M1C1-R4[d]	290	422	545	581		1000	4.58	4.08	1.06
M1C1-PC4[d]	400			588	663	996	3.83	3.25	0.85

[a] In the range 273−1073 K. [b] In the LTR (273−723 K). [c] In the LTR (273−723 K) [d] Pretreated in situ at 673 K for 30 min in oxygen flow (30 stp cm^3·min^{-1}).

of variation of the Mn loading (9−33 wt %), this represents a very remarkable characteristic of the new synthesis route. On the other hand, with a Mn/Ce surface value (0.42) threefold lower than the counterpart M1C1-R4 sample (Figure 7), XPS analysis provides evidence of a much lower dispersion of the active MnO_x phase in the counterpart M1C1-PC4 system, a consequence of deeply different structure and morphology.

(4) Redox Properties. According to literature findings indicating close relationships among dispersion, AON of Mn ions, and catalyst reducibility,[4,6−8,11−13,21,25,30] TPR results collected in Figure 8 and Table 2 confirm that the preparation method accounts also for evident changes in the redox behavior of the $MnCeO_x$ system. Because all the TPR profiles are characterized by two regions of hydrogen consumption spanned in the ranges 273−723 K (LTR) and 773−1073 K (HTR), relative to the reduction of active phase ($MnO_x \rightarrow MnO$) and ceria carrier ($CeO_2 \rightarrow Ce_2O_3$), respectively,[5−7,10−12,16,20,25,30] these data provide evidence of the fact that the preparation method (Figure 8A) has also a relevant influence on the reduction of the active phase in qualitative and quantitative terms. The spectrum of the coprecipitated system consists of two resolved peaks in the LTR centered at 588 and 673 K with an onset temperature of reduction of 400 K (LTR), associated with the reduction of poorly crystalline MnO_2 and Mn_2O_3 species, respectively.[25,30] A quite smaller band of H_2 consumption at $T > 773$ K, with a maximum at approximately 1000 K (HTR), is typical of the reduction of subsurface Ce^{4+} ions.[5−7,10,11,16,20,25] The total hydrogen consumption equals approximately 3.3 mmol/g, while that in the range 273−723 K accounts for a H_2/Mn ratio equal to 0.70. Markedly shifted to lower temperature ($T_{0,red}$, 365 K), the reduction profile of the "redox-precipitated" M1C1-R4 system (Figure 8A) shows in the LTR a "narrower" band of H_2 consumption, bearing two close and poorly resolved maxima at 545 and 591 K, respectively, and a slighter reduction peak of the ceria matrix (HTR). Overall, a larger hydrogen consumption (3.60 mmol/g) mirrors an increase of the H_2/Mn ratio (0.85), consistent with the enhanced MnO_x dispersion.[6−8,10,12]

Analogous structural properties account for a minor influence of the manganese loading on the reduction features of the "redox-precipitated" system (Figure 8B). The hydrogen consumption rises regularly with the Mn/Ce ratio from 2.3 to 5.27 mmol/g$_{cat}$, while a steady decrease of the H_2/Mn ratio (Table 2) signals a decrease in the extent of reduction of cerium ions in the LTR.[5−8] Overall, these data indicate an enhanced mobility and availability of catalyst lattice oxygen due to a high dispersion of active phase.[6−8,10] Hence, the "redox-precipitated" catalysts miss the component at approximately 670 K relative to Mn_2O_3 species while, associated with the reduction of "isolated" Mn^{4+} ions, the peak at

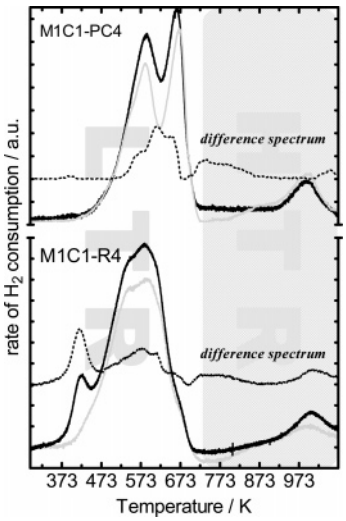

Figure 9. Influence of the pretreatment in situ (black lines) in oxygen at 673 K on the reduction pattern of the M1C1-R4 and M1C1-PC4 catalysts. Gray lines are the profiles of untreated samples (see Figure 8A), while the dashed black lines are the difference spectra (e.g., TPR profile of the pretreated sample subtracted from that on the untreated one).

545 K is nearly absent in the spectrum of the coprecipitated system owing to a much lower active phase dispersion.[15,25,30]

Catalyst treatment in a pure oxygen flow (673 K) before TPR analysis enhances further the different redox behaviors of the $MnCeO_x$ systems obtained via the above synthesis routes. The TPR profiles of the "pretreated" M1C1-PC4 and M1C1-R4 samples, compared in Figure 9, display in fact that the rate of hydrogen consumption of the "redox-precipitated" catalyst increases markedly in the LTR due to the appearance of a new reduction band in the range 323-423 K (see difference spectrum), lowering the onset temperature for reduction (290 K) by approximately 100 K with respect to the untreated sample (Table 2). The new reduction component(s) (T_{M0}, 422 K) along with a slightly larger intensity of those relative to the reduction of the active phase, corresponds to much larger overall consumption (4.58 mmol/g_{cat}) and H_2/Mn (1.06) values. The profile of the coprecipitated sample displays instead minor, if any, qualitative differences in the LTR, as only an increased intensity of the same reduction components (see difference spectrum) signals a bigger consumption and a moderate increase of the H_2/Mn ratio to 0.85 (Table 2).

These findings denote a quite different surface affinity toward molecular oxygen, still related to the different structural and textural properties. In fact, the new component indicates the formation of huge amounts of quite "reactive" surface oxygen species (i.e., O_2^-, O_2^{2-}, O^-, etc.), markedly enhancing the oxidizing strength of the system in a temperature range suitable for many catalytic applications.[3−22,25] This can be explained taking into account that the oxidative treatment prompts the removal of water molecules from the coordinative shell of "isolated", highly unsaturated (CUS) Mn^{4+} ions enabling the adsorption/activation of molecular oxygen at the surface of "redox-precipitated" catalysts. Evidently, this effect is almost negligible for the coprecipitated system because of two concomitant negative effects linked to a much lower dispersion of the active phase. Namely, low "exposure" of manganese ions in MnO_x species and a much lower degree of surface coordinative unsaturation depress the affinity of the coprecipitated system toward gas-phase oxygen.

Conclusions

An original synthesis procedure, driving redox-precipitation reactions among various Mn and Ce precursors, leads to highly dispersed and homogeneous $MnCeO_x$ catalysts.

Irrespective of manganese loading (9−33 wt %), the redox-precipitation route ensures invariable larger surface area exposure and dispersion of the active phase.

A "monolayer" dispersion of the active phase enhances the redox behavior and the surface affinity to oxygen of "redox-precipitated" $MnCeO_x$ catalysts in comparison to conventional coprecipitated systems.

The redox-precipitation route could provide new perspectives on the synthesis of molecularly structured materials for catalytic applications.

CM070198N